




# Effect of Nb on improving the impact toughness of Mo-containing low-alloyed steels

H. C. Wang<sup>1,\*</sup> , C. Somsen<sup>1</sup>, Y. J. Li<sup>2</sup>, S. G. Fries<sup>3</sup>, E. Detemple<sup>4</sup>, and G. Eggeler<sup>1</sup>

<sup>1</sup>Institute for Materials, Ruhr-Universität Bochum, 44801 Bochum, Germany

<sup>2</sup>ZGH, Ruhr-Universität Bochum, 44801 Bochum, Germany

<sup>3</sup>ICAMS, Ruhr-Universität Bochum, 44801 Bochum, Germany

<sup>4</sup>Department of Heavy Plate Research, AG der Dillinger Hüttenwerke, 66763 Dillingen/Saar, Germany

Received: 2 November 2018

Accepted: 18 January 2019

Published online:  
22 January 2019

© Springer Science+Business  
Media, LLC, part of Springer  
Nature 2019

## ABSTRACT

The microalloying of low-alloyed steels with Nb can improve the strength-to-toughness balance. Such an effect of Nb is usually ascribed to the refinement of the grain structure occurring in the austenite regime during hot forming. In the present work, we report that Nb enhances the impact toughness of a low-alloyed Cr–Mo steel by a mechanism which has not been appreciated so far. The lower impact toughness in the Nb-free Cr–Mo steel is due to segregation of Mo to boundaries, which facilitates the formation of fine Mo-rich  $\xi$ -phase carbides lining up along the boundaries. This further promotes the nucleation and propagation of microcracks. The addition of Nb leads to the formation of Mo-enriched NbC particles. The interfaces between these particles and the matrix supply new preferential sites for precipitation of Mo-rich  $\xi$ -phase carbides upon subsequent tempering. In this way, Nb additions result in a decrease of Mo segregation to boundaries, significantly reducing the precipitation of  $\xi$ -phase carbides on grain boundaries, thus leading to improved impact toughness. In addition to the classical microstructural explanation (grain size effect), this chemical role of Nb sheds new light on the design strategies of advanced low-alloyed steels with optimized strength-to-toughness ratios.

## Introduction

Niobium (Nb) as a microalloying element is added to low-alloyed steels to improve processing, microstructures and mechanical properties [1, 2]. In particular, Nb improves the strength-to-toughness

balance. This has been ascribed to the refinement of the grain structure occurring in the austenite regime during hot forming [3–14]. The solute drag effect of Nb atoms in solid solution [3–6] and/or the grain boundary pinning effect of niobium carbonitrides under typical recrystallization conditions [5–13] have been invoked to explain the effect of Nb. For certain

Address correspondence to E-mail: hongcai.wang@rub.de

classes of high-strength low-alloyed steels, additional quenching and tempering (Q&T) heat treatments after rolling have proven to be beneficial. The Q&T treatments lead to the formation of various types of carbides, such as  $M_2C$ ,  $M_3C$ ,  $M_7C_3$  and  $M_{23}C_6$ , where M stands for the metallic elements in the carbides. Different carbides form at different temperatures and appear at different microstructural locations, such as prior austenite grain boundaries (PAGB), micrograin boundaries [15] in fully bainitic (B) regions or boundaries between fully bainitic and fully ferritic (F) regions. Depending on their types and distributions, carbides can strongly influence the material toughness [16–19]. It has been shown that brittle cleavage failure can be initiated by the formation of microcracks associated with carbide fracture [20, 21]. Carbide-decorated grain boundaries have been suggested to represent easy crack propagation paths [22]. Molybdenum (Mo) is a strong carbide former and also known to segregate to grain boundaries during quenching and tempering [23–27], where it can form fine Mo-rich carbides lining up along the boundaries and further promote the nucleation and propagation of microcracks. Nb is also a strong carbide former. NbC particles have a high thermodynamic stability. It was also reported that NbC can incorporate other elements such as Mo [28–30]. However, the influence of Nb on the carbide precipitation process in Mo-containing steels during Q&T treatments has so far remained unclear.

The present work studies the effect of Nb on yield strength and impact toughness by comparing two low-alloyed steels with and without Nb addition after quenching and after tempering (Q and T states). The results show that the presence of Nb significantly improves impact toughness without compromising strength. The corresponding microstructure and local alloy compositions of the materials were characterized using analytical transmission electron microscopy (TEM) in combination with atom probe tomography (APT). The thermodynamic stabilities of carbides were analyzed in light of Thermo-Calc [31, 32] predictions. We show how the presence of Nb strongly alters the composition and distribution of  $\xi$ -phase carbides along internal interfaces during Q&T treatments and thus impacts mechanical properties. These new findings supplement the classical grain refinement effect of Nb on improving the impact toughness and provide new insights for the designs

of steels with optimum toughness-to-strength balance.

## Experimental procedure

### Materials

The specimens investigated in the present work were taken from 150-mm-thick rolled plates at a quarter position (38 mm underneath the plate surface). Their chemical compositions in wt% are Fe–0.13C–0.53Si–0.56Mn–0.17Ni–1.39Cr–0.57Mo (referred to as CrMo steel) and Fe–0.11C–0.53Si–0.58Mn–0.18Ni–1.40Cr–0.58Mo–0.021Nb (referred to as CrMoNb steel), respectively. The two materials differ in Nb content; the concentrations of the other alloying elements are nearly the same. After continuous casting, the two steels were reheated to 1200 °C followed by hot rolling at about 1000 °C (above non-recrystallization temperature and thickness reduced from ~ 800 mm to ~ 150 mm). Afterward, the steels were austenitized at 950 °C for 1 h, followed by water quenching (cooling rate ~ 2 °C/s; material state Q). Subsequently, the materials were tempered at 700 °C for 30 min (material state referred to as QT). Alternative tempering was also performed at higher temperatures, at 750 °C for 5 min for CrMo and at 740 °C for 5 min for CrMoNb steel, respectively (material states referred to as QT+). A schematic diagram of the complete processing route can be found in Supplementary materials (Figure S1). The three material states investigated in the present work are listed in Table 1.

Thermodynamic calculations were performed using the commercial CALPHAD software Thermo-Calc in combination with the TCFE9 database [31, 32]. The relative stabilities of different metastable carbides were evaluated by suspending one or more phases in the equilibrium calculations.

### Experimental techniques

The prior austenite grain (PAG) sizes of the two steels in their Q states were measured using optical microscopy in combination with image analysis. The samples were prepared by mechanical polishing (down to 1  $\mu$ m diamond suspension) followed by etching for about 1 min in an etchant consisting of 100 ml saturated aqueous picric acid, 1 g copper

**Table 1** Material states investigated in the present work

Steels	Q	QT	QT+
CrMo	Quenched	Quenched and tempered at 700 °C for 30 min	Quenched and tempered at 750 °C for 5 min
CrMoNb	Quenched	Quenched and tempered at 700 °C for 30 min	Quenched and tempered at 740 °C for 5 min

chloride and 1 ml washing detergent. The PAG sizes were determined using a line interception method in regions containing approximately one hundred grains.

From each steel in the QT and QT + states, nine standard Charpy impact specimens (36 specimens in total, 10-mm-square bar, length: 55 mm, 2 mm V-notch geometry) were tested in the temperature range between  $-10$  °C and  $-40$  °C. Cylindrical tensile test pieces were machined with a gauge diameter of 12.5 mm and a gauge length of 65 mm. Displacement-controlled tensile tests were performed at room temperature according to ASTM A370 [33].

TEM was performed using an FEI Tecnai Super-twin F20 equipped with a field emission gun operating at 200 kV and an energy-dispersive X-ray analysis (EDS) system from EDAX<sup>®</sup>. Thin foils were prepared by grinding 3-mm-diameter disks to a thickness of 50  $\mu\text{m}$ , followed by twin-jet electropolishing in a TenuPol-5 (from Struers). Good thinning conditions were achieved using an electrolyte consisting of 70 vol% methanol, 20 vol% glycerin and 10 vol% perchloric acid, flow rates between 15 and 20 and voltages of  $30 \pm 5$  V at  $-11$  °C. Carbides were identified using selected area electron diffraction (SAED, larger particles) and convergent beam electron diffraction (CBED, smaller particles). Carbide sizes were evaluated from scanning transmission electron (STEM) micrographs using the image analysis software ImageJ [34]. The diameter of particles was determined by taking the mean value of the projected maximum and minimum values. The average size of a particle family,  $\bar{d}$ , was then calculated as the average value of 10–300 particles, depending on the particle family. The particle number density of each particle family,  $\rho_n$ , was obtained by dividing the particle number by the area of the sampling field. A detailed description of the quantitative metallographic procedure used in the present work has been recently documented [35].

Using a dual-beam focused ion beam (FIB)/SEM instrument (FEI Helios G4 CX), APT needle-shaped

specimens were fabricated by a standard lift-out procedure described in [36]. APT investigations were performed using a local electrode atom probe (LEAP 5000 HR, Cameca Instruments) in voltage mode at 70 K, using a pulse fraction of 20%, a pulse repetition rate of 200 kHz and a detection rate of 0.01 atoms per pulse. The APT data were reconstructed and analyzed using the commercial IVAS 3.6.14 software [25, 37].

## Results

### Prior austenite grain (PAG) sizes of the quenched steels

The optical micrographs in Fig. 1 show the PAG boundaries in both steels after quenching. The average PAG size measured using the linear interception method was  $30 \pm 20$   $\mu\text{m}$  in both steels. These findings suggest that the addition of Nb has no strong influence on the PAG size for the steels in the present study.

### Mechanical properties

The tomography of fractured specimens was subjected to SEM observations, which exhibits intergranular facets with very little associated plastic deformation in both steels (see Supplementary

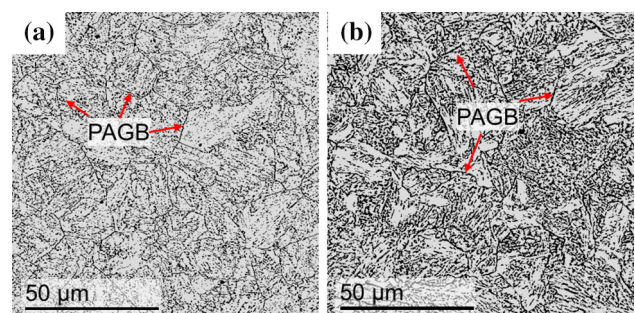


**Figure 1** Optical micrographs showing the prior austenite grains of the two steels in their Q states. **a** CrMo steel. **b** CrMoNb steel.

Figure S2). Figure 2 summarizes mechanical data which were obtained for the two steels investigated in the present work in their tempered states (QT and QT +). The tempered QT states show similar yield stresses close to 500 MPa (Fig. 2a). The alternative tempering heat treatment (QT + states) results in a decrease of yield stress. This decrease in yield stress is less pronounced for the CrMoNb steel (Fig. 2a). Figure 2b shows that the QT + heat treatment is beneficial. It results in significantly higher Charpy impact energies and thus higher impact toughness values in the whole temperature range from  $-40$  to  $-10$  °C (Fig. 2b). It is important to highlight that the CrMoNb steel has a significantly higher impact toughness at  $-40$  °C (Fig. 2b). While this advantage of the CrMoNb steel is no longer observed at  $-10$  °C, it has the advantage of a higher strength at the same impact toughness. The mechanical data presented in Fig. 2 clearly prove the beneficial effect of Nb in low-alloyed ferritic steels.

## Microstructure evolution

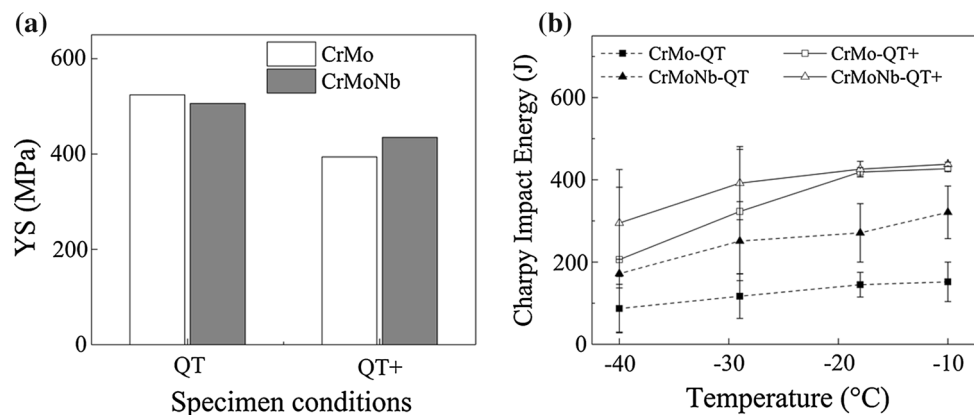
### Morphology and Mo-enriched NbC carbide in the Q state

Figure 3 shows the microstructure characterized by SEM and TEM for the two quenched steels, CrMo-Q and CrMoNb-Q. The microstructure of both materials consists of regions without clear features which are ferritic regions (F, dark) and regions with a more complex structure which are referred to as bainitic regions (B, complex microstructure). TEM investigations show that in the CrMo-Q steel, the grain boundaries are decorated by elongated  $M_3C$  particles (Fig. 3c) (for identification, see Fig. 3d).  $M_3C$  is also the only type of particle observed in CrMo-Q at grain boundaries. However, such particles are absent in

CrMoNb-Q. The microstructure of CrMoNb-Q shows dispersed small islands in a ferritic matrix, as indicated by the arrows in Fig. 3f. These islands were identified by electron diffraction as regions containing either austenite or a martensite/austenite mixture (Fig. 3g). They are referred to as M-A islands. In the matrix of CrMoNb-Q, as shown in the STEM micrograph of Fig. 3g, two arrays of small bright nanoparticles are observed (highlighted by arrows). The first array consists of a small number of particles which are about 50 nm in size. There are significantly more nanoparticles in the second array, which are more closely spaced and about 10 nm in size (Fig. 3g). The particles in both arrays are identified as NbC carbides by EDS analysis in Fig. 3i and by high-resolution TEM image analysis in Fig. 3j, k.

The distribution of relevant elements in a small volume of CrMoNb-Q was analyzed by APT (Fig. 4). In Fig. 4a, the blue-colored isoconcentration surfaces plotted at 0.5 at% NbC reveal the presence of Nb- and C-rich particles. The local rectangle in Fig. 4a represents a region which was analyzed further. The elemental distributions of C, Fe, Mo and Nb are shown in Fig. 4b. It can be clearly seen that the central particle is enriched with C, Mo and Nb. Figure 4c shows the average proximity histograms across the three NbC/matrix interfaces as marked with black arrows in Fig. 4a. The error bars represent the mean deviation from the mean value. An enrichment of Mo in the NbC particles is evident. However, concentrations of Nb and C are much lower than expected for NbC particles. Since the NbC particles obtained in the measured volume are very small ( $< 10$  nm), a “local magnification effect” [38], which causes trajectory overlaps of ions, cannot be avoided. Because of trajectory overlaps, Fe ions coming from the

**Figure 2** Results of the mechanical properties. **a** Yield strength (YS) in the two steels in the two tempered states (QT and QT +). **b** Charpy V-notch impact energy of the two steels in the two tempering conditions (QT and QT +) in the temperature range from  $-40$  to  $-10$  °C.



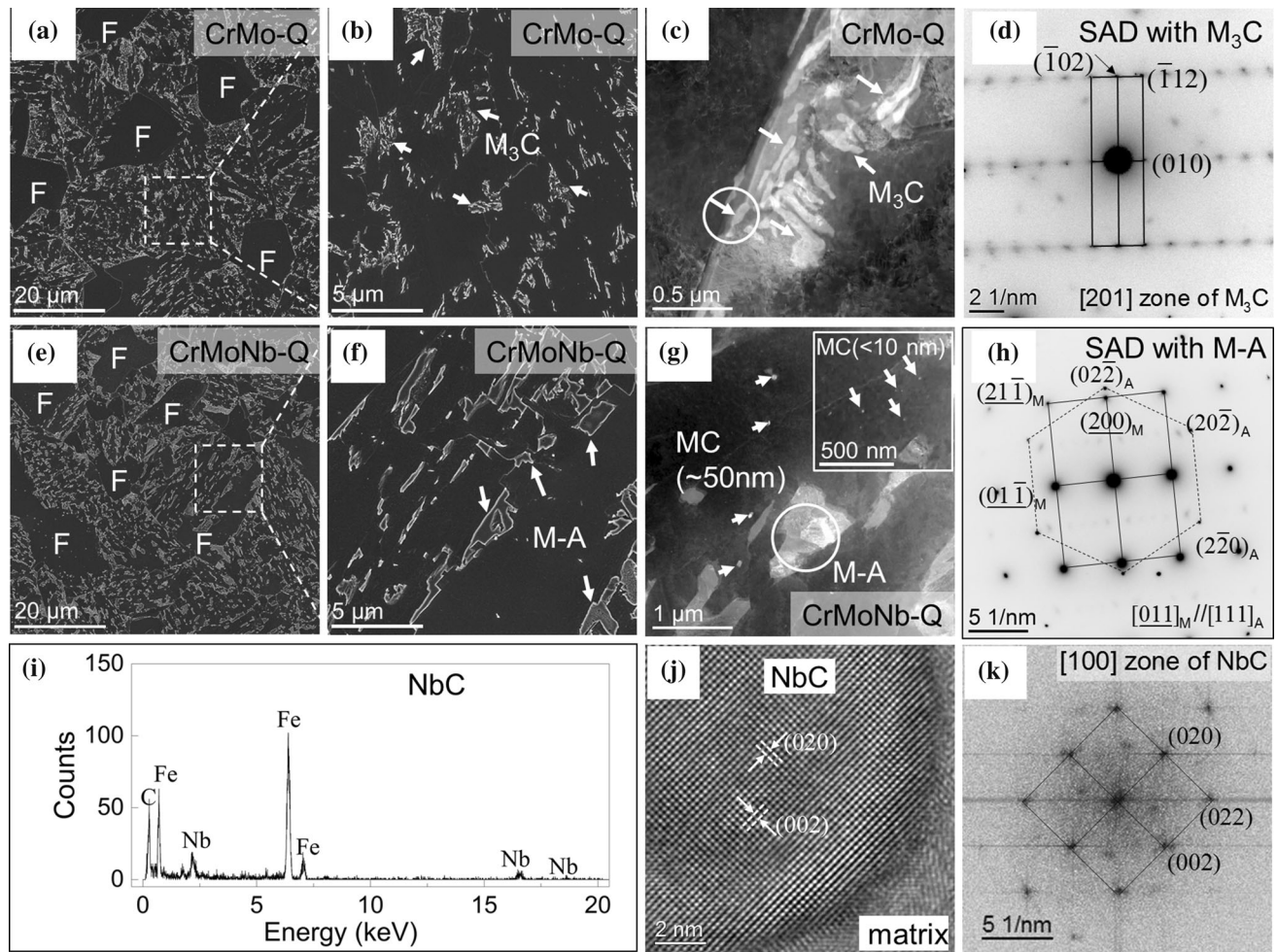


**Figure 3** Scale bridging comparison of CrMo-Q and CrMoNb-Q microstructures. **a–b** SEM micrographs of CrMo-Q showing the presence of ferritic (F) and bainitic regions. **c** STEM micrograph of  $M_3C$  particles at a grain boundary in CrMo-Q. **d** SAED pattern of the encircled  $M_3C$  particle from Fig. 3c with zone axis  $[201]_{M_3C}$ . **e–f** SEM micrographs of CrMoNb-Q showing similar F-regions

and 1- $\mu$ m-sized M-A islands. **g** STEM images showing 50-nm- and less than 10-nm-sized NbC particles (white arrows). **h** SAED pattern from M-A island encircled in Fig. 3g, orientation relationship  $[011]_M//[111]_A$ . **i** EDX spectrum of a NbC particle. **j** High-resolution TEM image from zone axis  $[100]_{NbC}$ . **k** The corresponding FFT pattern of (j).

surrounding matrix fall in the precipitate region during the APT measurements. As a result, the elemental concentrations in small particles can be significantly underestimated [38].

### *$\xi$ -phase carbide precipitation in the QT state*

The microstructures of the two steels after tempering at 700 °C for 30 min are shown in Fig. 5. While the F-regions without clear features and the bainitic regions with complex substructures (as observed in the Q state) remain the dominant microstructural features after tempering (see Fig. 5a for CrMo-QT and e for CrMoNb-QT), further carbide precipitation

has occurred. During tempering, the M-A regions in CrMoNb-QT (Fig. 3f, g) have decomposed into ferrite with carbides (Fig. 5e, f). The STEM micrographs for the representative areas of the B-regions in the two steels (Fig. 5b, f, respectively) show similar microstructural features. In both steels, particles have formed at/near grain boundaries. The majority of these carbides are of type  $M_3C$ .

When the areas highlighted in Fig. 5b, f are further investigated at higher magnification, striking differences between CrMo-QT and CrMoNb-QT become apparent: *First*, fine NbC particles of 10 nm in size are observed in CrMoNb-QT (Fig. 5g). *Second*, a large number of small  $\xi$ -carbides (for identification, see

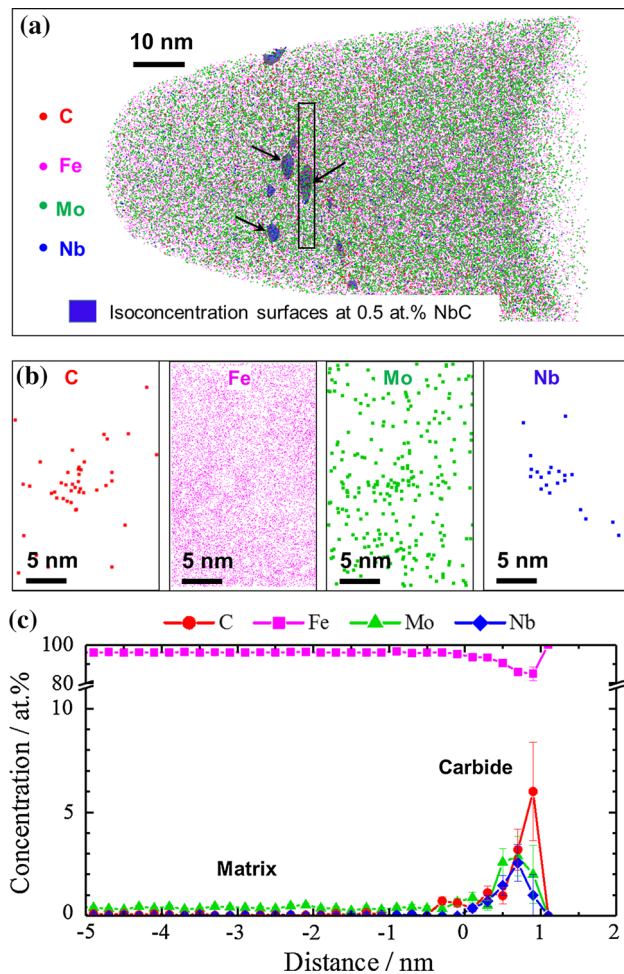


**Figure 4** APT analysis of CrMoNb-Q. **a** Distribution of the C (red), Fe (pink), Mo (green) and Nb (blue) atoms. Regions identified by blue-colored isoconcentration surfaces for 0.5 at% NbC are Mo-enriched NbC. **b** Distribution of the atoms in the selected rectangle ( $28 \times 18 \times 3 \text{ nm}^3$ ) marked in **(a)** showing enrichment of Mo in the NbC particle. **c** Proximity histograms of C, Fe, Mo and Nb obtained from three interfaces marked by arrows in **a**.

Fig. 5i) typically line up along boundaries in CrMo-QT (Fig. 5c). Such fine  $\xi$ -phase carbides are also present at the boundaries between B- and F-regions in CrMo-QT (Fig. 5d). In contrast, only few particles are observed at grain boundaries in CrMoNb-QT and some of these carbides are  $M_2C$  (for identification, see Fig. 5j) instead of  $\xi$ -carbide (Fig. 5g). *Third*, in CrMo-QT, a few  $M_{23}C_6$  particles are observed at grain boundaries within the selected B-region (Fig. 5c) (for identification, see Fig. 5k). No  $M_{23}C_6$  particles can be found in B-regions of CrMoNb-QT (Fig. 5f, g). These are only observed at grain boundaries or triple

junctions where F- and B-regions are present (Fig. 5h).

Precipitation in the F-regions due to tempering is different for the two steels. In the F-regions of CrMoNb-QT, fine NbC particles ( $\sim 10 \text{ nm}$  in diameter) are present (arrows in Fig. 6a) while no particles are found in the F-regions of CrMo-QT. In addition, a large population of  $\xi$ -phase carbides (in a few cases, Mo-rich  $M_2C$  particles) are precipitated at the interface between NbC particles and matrix. This results in the formation of composite-particles, which show a bright contrast in Fig. 6a. Similar composite particles are also found in the B-region of CrMoNb-QT, and they are composed of  $M_2C$  particles and NbC particles (Fig. 6b). The composite character of these particles can be clearly resolved at higher magnifications (Fig. 6c) (upper image: F-region of CrMoNb-QT; lower image: B-region of CrMoNb-QT).

#### *Improved impact toughness by higher temperature tempering—the QT + state*

The QT + microstructures of both steels shown in Fig. 7 still reveal most of the features of the QT states (Fig. 5). Figure 7a shows an overview SEM micrograph of CrMo-QT +, and Fig. 7b and c shows STEM images of its B- and F-regions at a higher magnification. The corresponding images for the Nb-containing steel CrMoNb-QT + are shown in Fig. 7d–f. Four regions which are marked with numbers in Fig. 7b, c (CrMo-QT +, locations 1 and 2) and in Fig. 7e, f (CrMoNb-QT +, locations 3 and 4) are further analyzed at higher magnifications in Fig. 7g (locations 1 and 2) and h (locations 3 and 4). It can be seen that there are less and larger carbides in the QT + states, as is obvious when comparing Figs. 5b and 7b (CrMo) and Figs. 5f and 7e (CrMoNb). Another important difference between the QT and the QT + material states is the disappearance of the  $\xi$ -phase carbides during tempering at higher temperatures (Fig. 7g, h). Only a few isolated large ones were occasionally found (Fig. 7c). In addition, in the QT + state, carbides of type  $M_7C_3$  are observed in both steels at grain boundaries (Fig. 7g, h).

#### *Size of carbides*

The particle sizes and their corresponding number densities in the two steels after tempering (QT) and

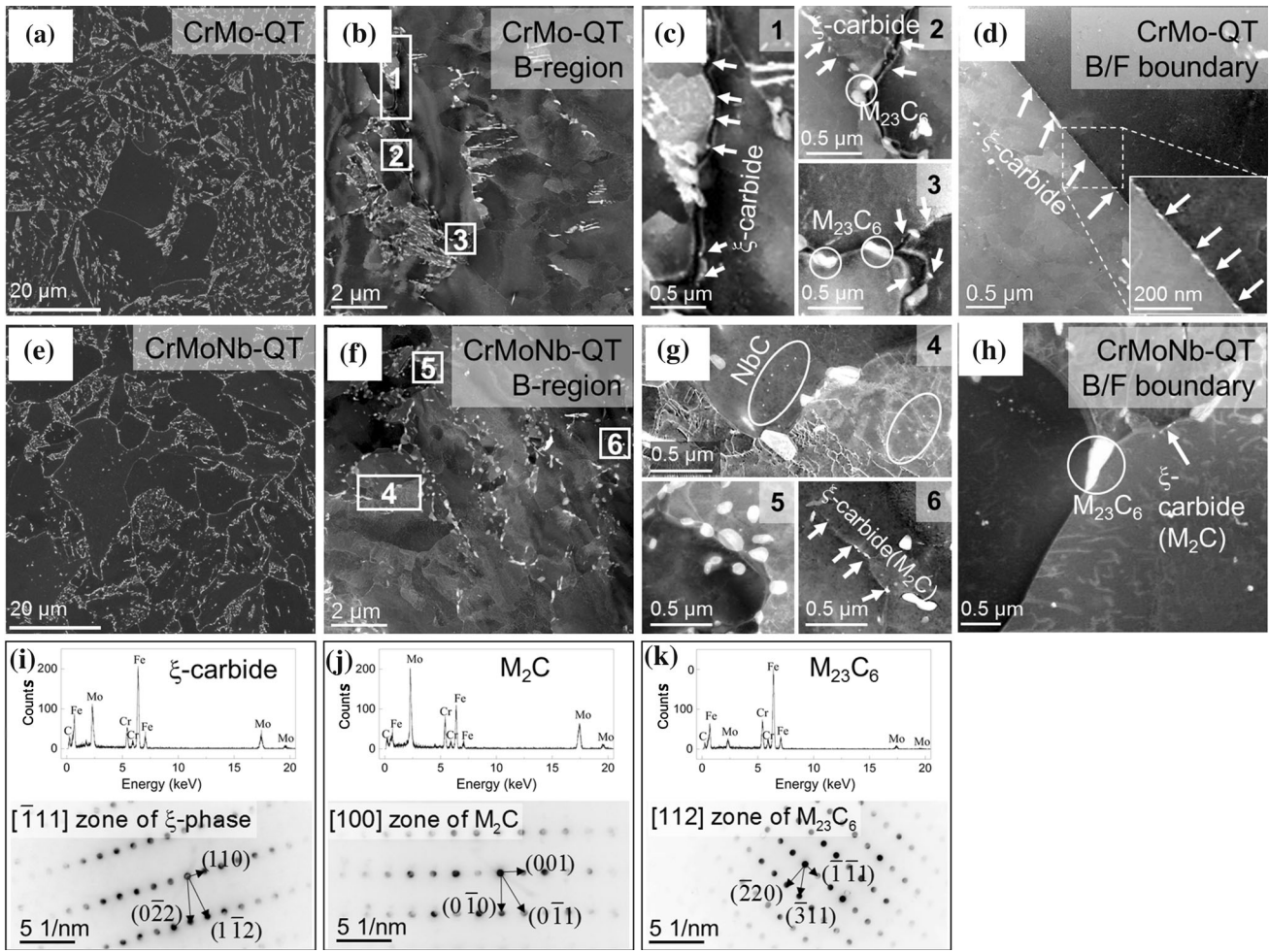


**Figure 5** Comparison of precipitates in CrMo-QT and CrMoNb-QT. **a** Low-magnification SEM overview of microstructure of CrMo-QT. **b** STEM image of a representative B-region from CrMo-QT. **c** Areas 1–3 highlighted in Fig. 6b enlarged. **d** A boundary between B- and F-regions in CrMo-QT decorated by fine  $\xi$ -phase carbides. **e** Low-magnification SEM overview of

microstructure of CrMoNb-QT. **f** STEM image of a representative B-region from CrMoNb-QT. **g** Areas 4–6 highlighted in Fig. 6f enlarged. **h** Large  $M_{23}C_6$  particle on triple point between two B- and one F-regions in CrMoNb-QT. There are no Mo-rich  $\xi$ -phase carbides (or  $M_2C$ ) on this boundary. **i–k** Typical EDX spectra with CBED patterns for  $\xi$ -phase carbide,  $M_2C$  and  $M_{23}C_6$ .

higher temperature tempering (QT +) are plotted in Fig. 8a, b, respectively. The NbC particles which form inside of grains in CrMoNb are smaller than all other carbides. They also show the highest number density. The  $M_{23}C_6$  particles, on the other hand, show the largest size but the lowest number density in both steels. Figure 8a also shows that with the exception of  $M_{23}C_6$ , the size of each individual type of particle in the QT + state is larger than that in the QT state. It is observed that the size of  $\xi$ -phase carbides in CrMoNb-QT is larger than that in CrMo-QT and further increases with tempering at higher temperature (QT +). The number density of  $\xi$ -phase carbides in CrMoNb is significantly lower than that in CrMo

and decreases with increasing tempering temperatures (Fig. 8b).

### Thermodynamic stability of carbides

Results for the dependence of equilibrium phase fractions on temperature evaluated by Thermo-Calc in the two steels are presented in Fig. 9. When all possible phases are considered (Fig. 9a, b),  $M_{23}C_6$ ,  $M_6C$  (both steels) and NbC (only CrMoNb) are found to be the stable phases. Particularly, NbC is stable up to about 1100 °C. When numerically suppressing the formation of the equilibrium phases  $M_{23}C_6$  and  $M_6C$ , the stability of metastable phases can be estimated. In this case,  $M_7C_3$  and  $M_2C$  replace  $M_{23}C_6$  while the

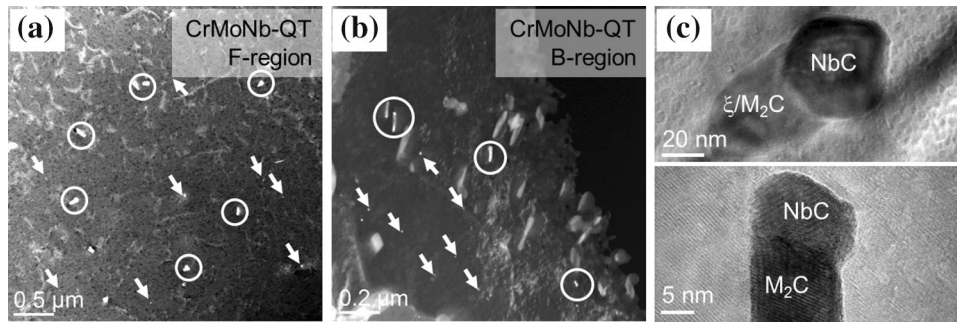


**Figure 6** STEM micrographs showing Mo-rich  $\xi$ -phase/ $M_2C$  particles forming on NbC particles in the **a** F-region and **b** B-region. The composite particles are highlighted by white circles.

White arrows indicating 10-nm-sized NbC. **c** TEM images taken at higher magnifications reveal the composite character, which is found in the F- (upper image) and in the B-region (lower image).

stability of NbC is not affected (Fig. 9c, d). Second, when  $M_7C_3$  is also suppressed, two additional carbide phases,  $M_3C$ - and  $\xi$ -phase, appear (Fig. 9e, f). Note that the solution temperature of the  $\xi$ -phase is about 750 °C in both steels.

## Discussion

### Stability of NbC and M-A islands

While it is generally believed that the beneficial effect of Nb on toughness in microalloyed steels is related to grain refinement [3–11], this cannot be confirmed by the results obtained in the present study. The present work suggests that Nb improves impact toughness by a mechanism which is related to the formation and stability of NbC. The Thermo-Calc results presented in Fig. 9 suggest that NbC is stable up to temperatures of about 1100 °C. Only a low number density of NbC particles ( $\sim 50$  nm) was found in the as-rolled state (results not shown in this paper). These relatively large NbC particles do not dissolve during the subsequent austenitization (at 950 °C) and quenching process. However, when the hot-deformed material is reheated to 950 °C during austenitization and then subjected to quenching, further NbC precipitation can occur. This is promoted by heterogeneous nucleation on dislocations [39, 40]. The newly formed NbC particles have a significantly smaller size ( $< 10$  nm), and their number density is high. In line with this view, the NbC particles after quenching shown in Fig. 3g belong to two different size classes. Moreover, the present study has shown that the addition of Nb also promotes the formation of M-A islands and suppresses

the precipitation of  $M_3C$  at grain boundaries during quenching (Fig. 3). The observations of two size classes NbC particles and M-A islands in Nb-steels and the suppression of  $M_3C$  precipitation by Nb are well in line with the recent work published by Hausmann et al., who studied the morphological change of retained austenite due to addition of Nb [41]. The formation of such M-A islands has been attributed to be related to the partitioning of carbon during phase transformations [41–46]. Further investigations are necessary to verify whether this applies to the current materials.

### $\xi$ -phase and impact toughness

Although the complex  $\xi$ -phase carbide has been known for several decades [47–51], it has not been considered whether or not it has an influence on mechanical properties. The present work suggests that the impact toughness of the two alloys is closely related to the precipitation and distribution of  $\xi$ -phase carbides. In contrast to CrMo-QT where a high number of  $\xi$ -phase carbides form on grain boundaries (Fig. 5c, d), only a few of such particles were observed in CrMoNb-QT (Fig. 5g, h). This is due to the fact that composite particles precipitated in the grain interior as shown in Fig. 6. Therefore, it can be suggested that crack propagation along boundaries is favored by the presence of  $\xi$ -phase carbides on these boundaries. This explains why CrMoNb-QT has a higher impact toughness than CrMo-QT (Figs. 2 and 8). In addition, tempering the materials at higher temperatures (QT +) leads to even less precipitation of  $\xi$ -phase (Fig. 7). Consequently, the impact toughness of QT + states is higher than that of QT states.



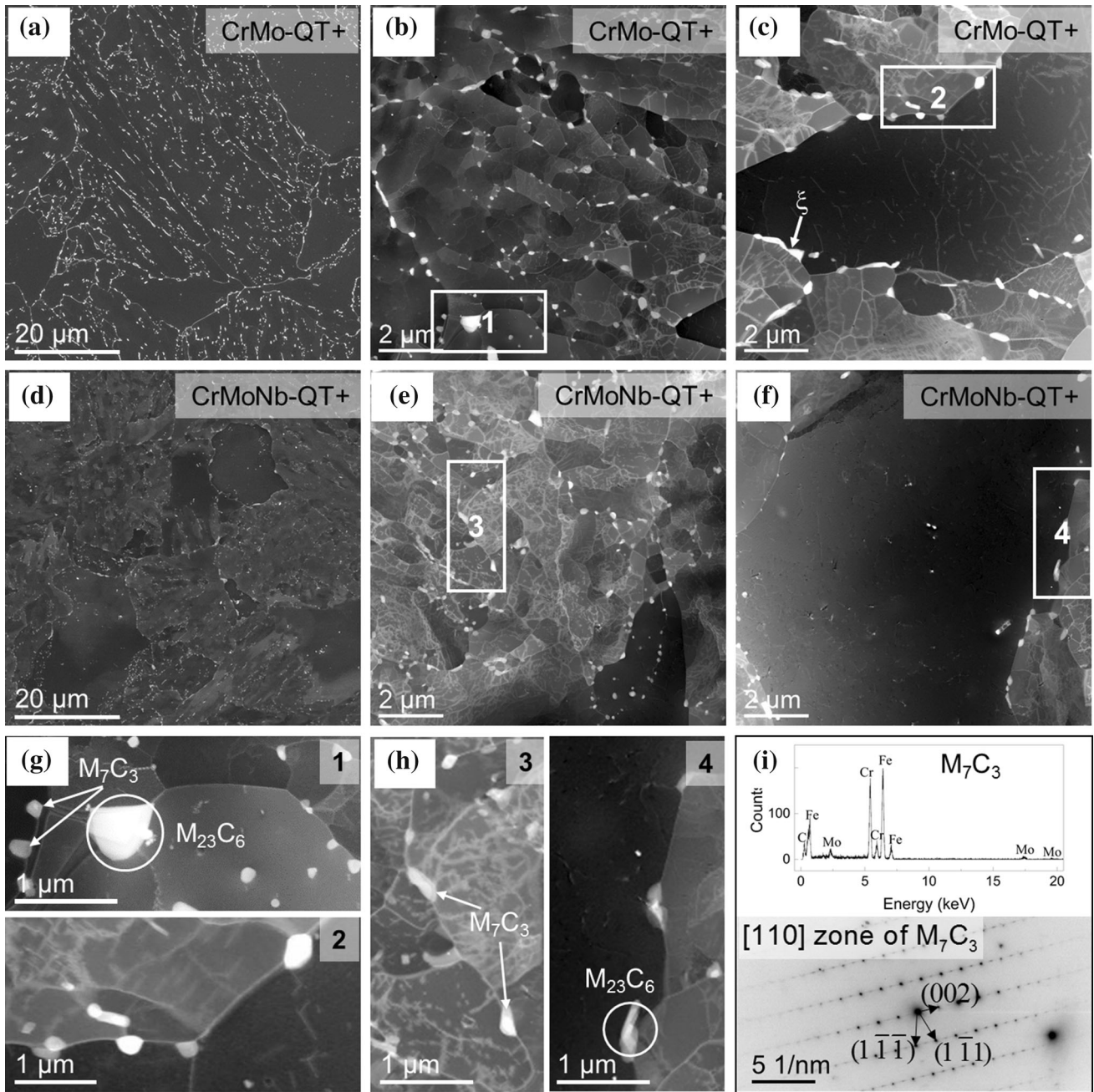


**Figure 7** Microstructural, chemical and crystallographic observations after higher temperature tempering (QT +). **a–c** SEM and STEM overview images of CrMo-QT +. **d–f** SEM and STEM overview images of CrMoNb-QT +. **g** Highlighted regions 1 and 2 from **b**, **c** (CrMo-QT +) at higher

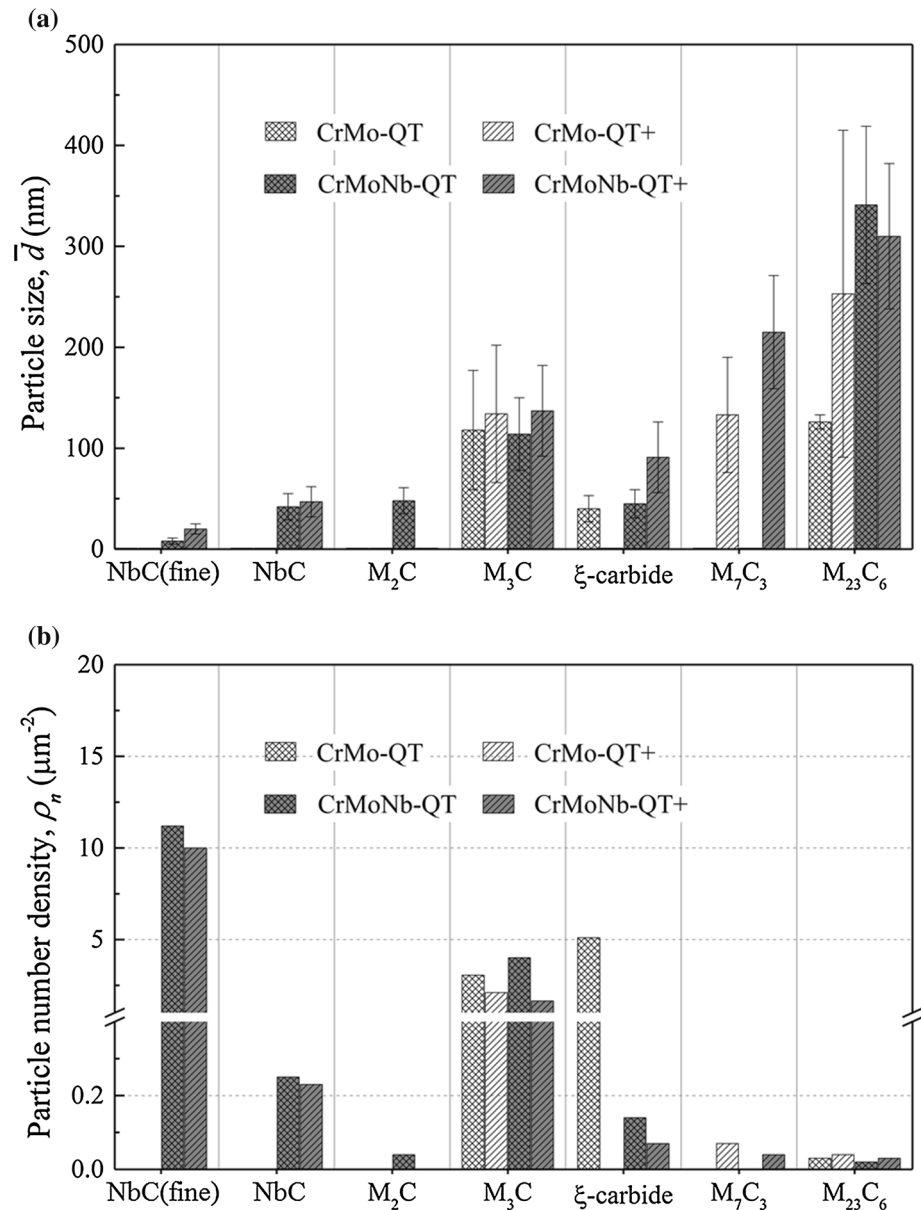
magnification. **h** Highlighted regions 3 and 4 from **e**, **f** (CrMoNb-QT +) at higher magnification. **i** Typical EDX spectrum and corresponding SAED pattern of a  $M_7C_3$  particle which formed during high-temperature tempering.

Detrimental effects of small boundary carbides on impact toughness have already been reported by Kuzin et al. [52] and Hong et al. [22]. Both conclude that the impact toughness decreases with an

increasing number of fine  $M_3C$  particles on grain boundaries and that the presence of fine particles on boundaries promotes intergranular fracture. The effect can be attributed to the mechanical

**Figure 8** Results on particle sizes and number densities.

**a** Average carbide sizes in the two tempered states (QT and QT +). **b** The corresponding number densities of each carbide in **a**.



consequences related to the presence of the boundary carbide itself, or, the physical/chemical nature of the carbide–matrix interfaces which facilitate the nucleation of cracks and their propagation along grain boundaries [20, 21, 53]. When stresses are transferred to non-deformable grain boundary carbides (either by grain boundary sliding or by localized deformation events), the carbide will crack or the carbide–matrix interface will cleave. Therefore, the high number of  $\xi$ -carbides may promote crack nucleation and reduce the work required for crack propagation [22, 53].

In the present study, the  $\xi$ -phase carbides precipitate preferentially at grain boundaries in CrMo-QT. Segregation of both C and Mo to grain boundaries occurs during quenching [23–27]. A higher Mo concentration at grain boundaries promotes the formation of  $\xi$ -phase [48, 51]. In contrast, the NbC particles in CrMoNb-Q were found to be enriched in Mo and a population of  $\xi$ -phase carbides form at the interface between NbC and matrix. As a result, segregation of Mo to grain boundaries is restricted, which consequently hinders the formation of  $\xi$ -phase carbides at grain boundaries. The thermodynamic calculations in

**Figure 9** Phase fractions as a function of temperature calculated with Thermo-Calc using the alloy compositions of CrMo and CrMoNb listed in Table 1. **a** CrMo—all possible phases considered. **b** CrMoNb—all possible phase considered. **c** CrMo— $M_{23}C_6$  and  $M_6C$  suppressed. **d** CrMoNb— $M_{23}C_6$  and  $M_6C$  suppressed. **e** CrMo— $M_{23}C_6$ ,  $M_6C$  and  $M_7C_3$  suppressed. **f** CrMoNb— $M_{23}C_6$ ,  $M_6C$  and  $M_7C_3$  suppressed.

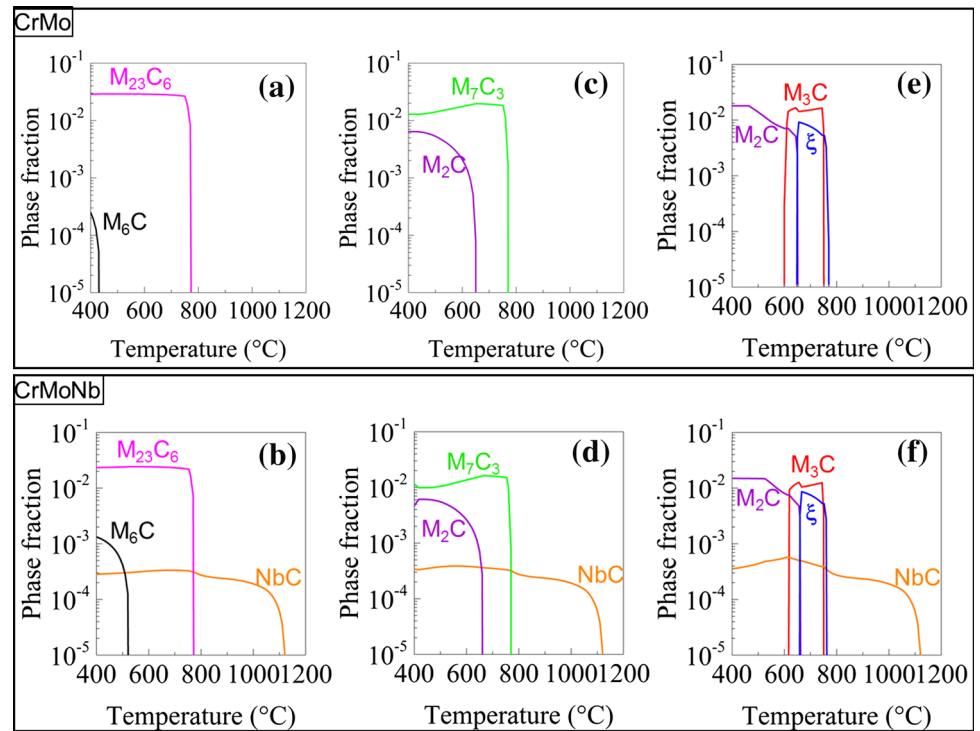
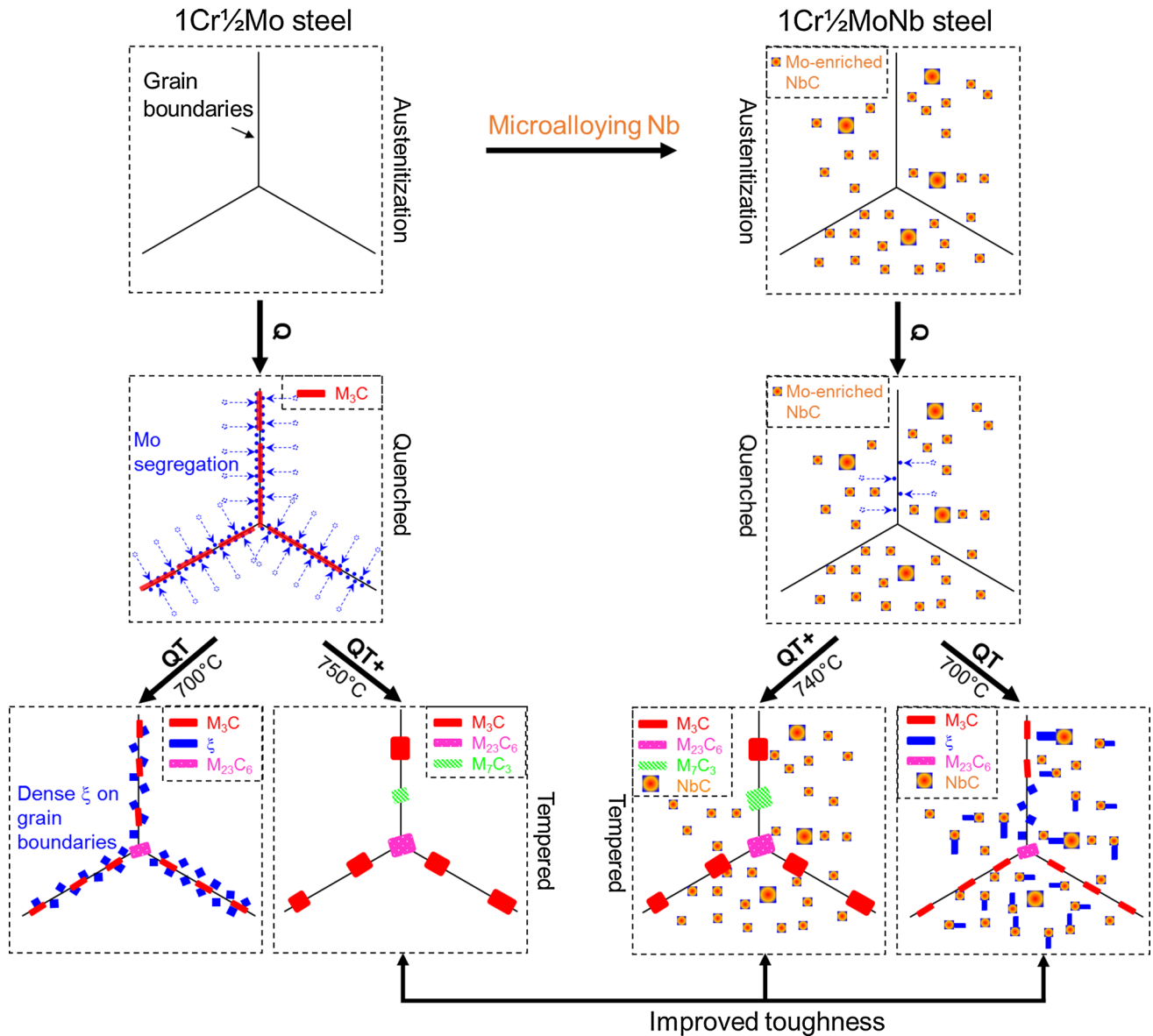


Fig. 9 show that the formation of  $\xi$ -phase occurs between 650 and 750 °C for the CrMo steel and between 680 to 750 °C for CrMoNb. The higher tempering temperatures (750 °C for CrMo and 740 °C for CrMoNb) used in the current study are near the upper limit of the metastable  $\xi$ -phase boundary. Therefore, very few  $\xi$ -phase carbides were observed in both steels in the QT + states.

### Mo segregation and the effect of Nb on improving impact toughness

The segregation of Mo to grain boundaries has been well studied [23, 24, 26, 27] in low-alloyed structural steels which were tempered after quenching. Such segregation has been reported to be beneficial because Mo is a known grain boundary strengthener [54, 55]. However, a higher Mo concentration also promotes the formation of Mo-rich carbides such as the  $\xi$ -phase carbides at grain boundaries in the present study [48, 51]. The formation of Mo-rich carbides on grain boundaries not only increases the probability for crack nucleation and propagation, but also counteracts the cohesion enhancement otherwise caused by the segregated Mo. The present study demonstrates that the impact toughness of high-strength Cr–Mo steels can be improved by either

microalloying the steels with Nb or by tempering at a higher temperature. In view of the different precipitation scenarios of carbides, this effect can be attributed to the prevention of the formation of fine  $\xi$ -phase particles at grain boundaries. In Fig. 10, the synergistic effect of Nb and Mo improving impact toughness during quenching and tempering is schematically illustrated based on the current experimental results. For the CrMo steel (left side of the figure), Mo strongly segregates to grain boundaries during quenching. This leads to the formation of fine  $\xi$ -particles in the subsequent tempering process and results in a decrease of impact toughness. However, such detrimental effect on the impact toughness can be mitigated by tempering at higher temperatures, where the fine  $\xi$ -particles no longer form. In the CrMoNb steel (right side of Fig. 10), the addition of Nb promotes the formation of NbC particles that incorporate Mo and supply additional nucleation sites for  $\xi$ -phase carbides in the grain interior. Mo segregation to grain boundaries is therefore hampered. As a consequence, less fine  $\xi$ -particles form at grain boundaries in the CrMoNb-QT. This explains why the Nb microalloyed CrMoNb steel has a higher impact toughness than the CrMo steel. Tempering the CrMo steels at higher temperature (QT +) also hampers the formation of  $\xi$ -carbide; therefore, the



**Figure 10** Schematic illustrations which show how Nb improves impact toughness. Left side: There is no Nb in the steel. Mo segregates to boundaries. This promotes the formation of fine  $\xi$ -phase carbides along boundaries which results in poor impact toughness. Tempering at higher temperatures removes the  $\xi$ -phase

impact toughness is similar to that of CrMoNb-QT + (Fig. 2b).

### Summary and conclusions

In the present work, a detailed microstructural study was performed on two Cr–Mo steels, one without and another with Nb additions. In Cr–Mo (no Nb), Mo segregates to boundaries which promotes the

and improves impact toughness. Right side: The steel contains Nb. NbC particles form at high temperatures and incorporate Mo. As a result, much less  $\xi$ -phase carbides form on grain boundaries during tempering and therefore better impact toughness is obtained.

formation of fine  $\xi$ -particles along grain boundaries. This can facilitate microcrack nucleation and propagation along the grain boundary. Adding Nb has a positive effect on impact toughness, which is not due to grain refinement. Instead, it was shown that in CrMoNb, the presence of Nb results in the formation of Mo-rich NbC particles. Therefore, significantly less Mo segregates to grain boundaries and the formation of fine  $\xi$ -particles is hampered. Their absence makes it more difficult for microcracks to nucleate/

propagate along grain boundaries, and as a result, better impact toughness values are obtained. Formation of fine  $\xi$ -particles can also be inhibited by applying higher tempering temperatures. This, however, can only be achieved at the expense of lower yield stresses.

## Acknowledgements

The authors are grateful to Ms. Klara Pohl for her help with chemical etching and grain size measurements.

**Electronic supplementary material:** The online version of this article (<https://doi.org/10.1007/s10853-019-03374-2>) contains supplementary material, which is available to authorized users.

## References

- [1] Deardo AJ (2003) Niobium in modern steels. *Int Mater Rev* 48:371–402
- [2] Baker TN (2016) Microalloyed steels. *Ironmak Steelmak* 43:264–307
- [3] Suehiro M, Liu Z-K, Ågren J (1996) Effect of niobium on massive transformation in ultra low carbon steels: a solute drag treatment. *Acta Mater* 44:4241–4251
- [4] Maruyama N, Smith GDW, Cerezo A (2003) Interaction of the solute niobium or molybdenum with grain boundaries in  $\alpha$ -iron. *Mater Sci Eng A* 353:126–132
- [5] Abad R, Fernández AI, López B, Rodríguez-Ibabe JM (2001) Interaction between recrystallization and precipitation during multipass rolling in a low carbon niobium microalloyed steel. *ISIJ Int* 41:1373–1382
- [6] Xiao F, Cao Y, Qiao G, Zhang X, Liao B (2012) Effect of Nb solute and NbC precipitates on dynamic or static recrystallization in Nb steels. *J Iron Steel Res Int* 19:52–56
- [7] Palmiere EJ, Garcia CI, DeArdo AJ (1996) The influence of niobium supersaturation in austenite on the static recrystallization behavior of low carbon microalloyed steels. *Metall Mater Trans A* 27:951–960
- [8] Misra RDK, Nathani H, Hartmann JE, Siciliano F (2005) Microstructural evolution in a new 770 MPa hot rolled Nb–Ti microalloyed steel. *Mater Sci Eng A* 394:339–352
- [9] Hutchinson CR, Zurob HS, Sinclair CW, Brechet YJM (2008) The comparative effectiveness of Nb solute and NbC precipitates at impeding grain-boundary motion in Nb steels. *Scr Mater* 59:635–637
- [10] Cao Y, Xiao F, Qiao G, Huang C, Zhang X, Wu Z, Liao B (2012) Strain-induced precipitation and softening behaviors of high Nb microalloyed steels. *Mater Sci Eng A* 552:502–513
- [11] Wu H, Ju B, Tang D, Hu R, Guo A, Kang Q, Wang D (2015) Effect of Nb addition on the microstructure and mechanical properties of an 1800 MPa ultrahigh strength steel. *Mater Sci Eng A* 622:61–66
- [12] Zhao H, Wynne BP, Palmiere EJ (2017) Effect of austenite grain size on the bainitic ferrite morphology and grain refinement of a pipeline steel after continuous cooling. *Mater Charact* 123:128–136
- [13] Larzabal G, Isasti N, Rodríguez-Ibabe J, Uranga P (2017) Evaluating strengthening and impact toughness mechanisms for ferritic and bainitic microstructures in Nb, Nb–Mo and Ti–Mo microalloyed steels. *Metals* 7:65
- [14] Chen Y-W, Huang B-M, Tsai Y-T, Tsai S-P, Chen C-Y, Yang J-R (2017) Microstructural evolutions of low carbon Nb/Mo-containing bainitic steels during high-temperature tempering. *Mater Charact* 131:298–305
- [15] Aghajani A, Somsen C, Eggeler G (2009) On the effect of long-term creep on the microstructure of a 12% chromium tempered martensite ferritic steel. *Acta Mater* 57:5093–5106
- [16] Bhadeshia HKDH (2001) Bainite in steels: transformations, microstructure and properties, 2nd edn. IOM Communications, London
- [17] Lee S, Kim S, Hwang B, Lee BS, Lee CG (2002) Effect of carbide distribution on the fracture toughness in the transition temperature region of an SA 508 steel. *Acta Mater* 50:4755–4762
- [18] Tanguy B, Besson J, Pineau A (2003) Comment on “Effect of carbide distribution on the fracture toughness in the transition temperature region of an SA 508 steel”. *Scr Mater* 49:191–197
- [19] Krauss G (2015) Steels: processing, structure, and performance, 2nd edn. ASM International, Materials Park
- [20] McMahon CJ, Cohen M (1965) Initiation of cleavage in polycrystalline iron. *Acta Metall* 13:591–604
- [21] Lindley TC, Oates G, Richards CE (1970) A critical of carbide cracking mechanisms in ferride/carbide aggregates. *Acta Metall* 18:1127–1136
- [22] Hong S, Lee J, Lee B-J, Kim HS, Kim S-K, Chin K-G, Lee S (2013) Effects of intergranular carbide precipitation on delayed fracture behavior in three TWinning Induced Plasticity (TWIP) steels. *Mater Sci Eng A* 587:85–99
- [23] Song S, Xu T (1994) Combined equilibrium and non-equilibrium segregation mechanism of temper embrittlement. *J Mater Sci* 29:61–66. <https://doi.org/10.1007/BF00356573>

- [24] Song S, Faulkner RG, Jiang H (1994) A new view on the temperature-time dependence of temper embrittlement. *J Mater Sci Lett* 13:1007–1009
- [25] Yuan L, Ponge D, Wittig J, Choi P, Jiménez JA, Raabe D (2012) Nanoscale austenite reversion through partitioning, segregation and kinetic freezing: example of a ductile 2GPa Fe–Cr–C steel. *Acta Mater* 60:2790–2804
- [26] Li YJ, Ponge D, Choi P, Raabe D (2015) Segregation of boron at prior austenite grain boundaries in a quenched martensitic steel studied by atom probe tomography. *Scr Mater* 96:13–16
- [27] Li YJ, Ponge D, Choi P, Raabe D (2015) Atomic scale investigation of non-equilibrium segregation of boron in a quenched Mo-free martensitic steel. *Ultramicroscopy* 159:240–247
- [28] Uemori R, Chijiwa R, Tamehiro H, Morikawa H (1994) AP-FIM study on the effect of Mo addition on microstructure in Ti–Nb steel. *Appl Surf Sci* 76–77:255–260
- [29] Lee W-B, Hong S-G, Park C-G, Park S-H (2002) Carbide precipitation and high-temperature strength of hot-rolled high-strength, low-alloy steels containing Nb and Mo. *Metall Mater Trans A* 33:1689
- [30] Enloe CM, Findley KO, Parish CM, Miller MK, De Cooman BC, Speer JG (2013) Compositional evolution of microalloy carbonitrides in a Mo-bearing microalloyed steel. *Scr Mater* 68:55–58
- [31] Thermo-Calc Software—Computational Materials Engineering. <http://www.thermocalc.com/>. Accessed 19 February 2018
- [32] Lukas HL, Fries SG, Sundman B (2007) Computational thermodynamics: the CALPHAD method. Cambridge University Press, Cambridge
- [33] ASTM A370-17 (2017) Standard test methods and definitions for mechanical testing of steel products. ASTM International, West Conshohocken
- [34] Schindelin J, Arganda-Carreras I, Frise E, Kaynig V, Longair M, Pietzsch T, Preibisch S, Rueden C, Saalfeld S, Schmid B, Tinevez J-Y, White DJ, Hartenstein V, Eliceiri K, Tomancak P, Cardona A (2012) Fiji: an open-source platform for biological-image analysis. *Nat Methods* 9:676–682
- [35] Wang H, Somsen C, Eggeler G, Detemple E (2018) Carbide types in an advanced microalloyed bainitic/ferritic Cr–Mo Steel—TEM observations and thermodynamic calculations. *Mater Werkst* 49:726–740
- [36] Saxey DW, Cairney JM, McGrouther D, Honma T, Ringer SP (2007) Atom probe specimen fabrication methods using a dual FIB/SEM. *Ultramicroscopy* 107:756–760
- [37] Integrated Visualization and Analysis Software (IVAS) for Atom Probe, Cameca Instr. <http://www.cameca.com/>. Accessed 19 February 2018
- [38] Philippe T, Gruber M, Vurpillot F, Blavette D (2010) Clustering and local magnification effects in atom probe tomography: a statistical approach. *Microsc Microanal* 16:643–648
- [39] Brito RM, Kestenbach H-J (1981) On the dispersion hardening potential of interphase precipitation in micro-alloyed niobium steel. *J Mater Sci* 16:1257–1263. <https://doi.org/10.1007/BF01033840>
- [40] Kwon O, DeArdo AJ (1991) Interactions between recrystallization and precipitation in hot-deformed microalloyed steels. *Acta Metall Mater* 39:529–538
- [41] Hausmann K, Krizan D, Spiradek-Hahn K, Pichler A, Werner E (2013) The influence of Nb on transformation behavior and mechanical properties of TRIP-assisted bainitic–ferritic sheet steels. *Mater Sci Eng A* 588:142–150
- [42] Misra RDK, Thompson SW, Hylton TA, Boucek AJ (2001) Microstructures of hot-rolled high-strength steels with significant differences in edge formability. *Metall Mater Trans A* 32:745–760
- [43] Zhao M, Yang K, Shan Y (2002) The effects of thermo-mechanical control process on microstructures and mechanical properties of a commercial pipeline steel. *Mater Sci Eng A* 335:14–20
- [44] Kong J, Zhen L, Guo B, Li P, Wang A, Xie C (2004) Influence of Mo content on microstructure and mechanical properties of high strength pipeline steel. *Mater Des* 25:723–728
- [45] Wang C, Wu X, Liu J, Xu N (2006) Transmission electron microscopy of martensite/austenite islands in pipeline steel X70. *Mater Sci Eng A* 438–440:267–271
- [46] Shanmugam S, Ramiseti NK, Misra RDK, Hartmann J, Jansto SG (2008) Microstructure and high strength–toughness combination of a new 700 MPa Nb-microalloyed pipeline steel. *Mater Sci Eng A* 478:26–37
- [47] Kuo K (1953) Carbides in Chromium Molybdenum and Tungsten Steels. *J Iron Steel Inst* 173:363–375
- [48] Sato T, Nishizawa T, Tamaki K (1962) Carbides in molybdenum steels. *Trans Jpn Inst Met* 3:196–202
- [49] Craig BD (1981) Direct observation of Fe<sub>2</sub>MoC carbides in a low alloy steel. *Scr Metall* 15:91–94
- [50] Rapposch M, Kostiner E, Wayne SF, Nowotny H (1985) The crystal structure of the molybdenum cementite Mo<sub>12</sub>Fe<sub>22</sub>C<sub>10</sub> ( $\xi$ -phase). *Monatshefte Für Chem* 116:1237–1245
- [51] Shtansky DV, Inden G (1997) Phase transformation in Fe–Mo–C and Fe–W–C steels—I. The structural evolution during tempering at 700 °C. *Acta Mater* 45:2861–2878
- [52] Kuzin OA, Kovrova TP, Meshcheryakova TM (1999) Influence of the carbide phase on fracture of improved steels. *Mater Sci* 35:220–224

- [53] Bhadeshia HKDH, Honeycombe RWK (2006) Steels: microstructure and properties. Butterworth-Heinemann, Oxford
- [54] Heo NH (1996) Grain boundary segregation and intergranular fracture in ferrite containing Mo, Si or Al. *Met Mater* 2:49–64
- [55] Geng WT, Freeman AJ, Wu R, Olson GB (2000) Effect of Mo and Pd on the grain-boundary cohesion of Fe. *Phys Rev B* 62:6208–6214